

A ROSAT Survey of Contact Binary Stars

M.T. Geske^{1,2}, S.J. Gettel¹, and T.A. McKay¹

ABSTRACT

Contact binary stars are common variable stars which are all believed to emit relatively large fluxes of x-rays. In this work we combine a large new sample of contact binary stars derived from the ROTSE-I telescope with x-ray data from the ROSAT All-Sky Survey (RASS) to estimate the x-ray volume emissivity of contact binary stars in the galaxy. We obtained x-ray fluxes for 140 contact binaries from the RASS, as well as 2 additional stars observed by the XMM-Newton observatory. From these data we confirm the emission of x-rays from all contact binary systems, with typical luminosities of approximately 1.0×10^{30} erg s^{-1} . Combining calculated luminosities with an estimated contact binary space density, we find that contact binaries do not have strong enough x-ray emission to account for a significant portion of the galactic x-ray background.

Subject headings: binaries: close – binaries: eclipsing – stars: activity – stars: variables: other – x-rays: stars

1. Introduction

Contact binaries are close binary stars that share a single convective envelope (Lucy 1968). They are very common systems; the most recent estimates find that they account for at least one out of every 500 main sequence stars (Rucinski 2002). W UMa type systems are the most common type, consisting of spectral types between F and K. In general, the systems show periods from 0.22-1.5 days, with the most common systems having periods in the range of 0.25-0.50 days. There is an incompletely understood period cutoff at 0.22 days (Stepień, et al. 2001; Rucinski 1992).

¹Department of Physics, University of Michigan, Ann Arbor, MI 48109

²mtgesk@umich.edu

Contact binary systems are expected to exhibit high levels of coronal x-ray emission as a result of their short periods. Observations have detected x-ray emissions from a majority of W UMa systems; Cruddace & Dupree (1984) detected x-ray emissions from 14 of 17 such systems in the Einstein Observatory IPC survey of W UMa systems. More recently, Stępień, et al. (2001) used the ROSAT All-Sky Survey to confirm x-ray emissions from 57 W UMa systems. A spectral survey of 8 W UMa systems was undertaken by McGale, et al. (1996), which found the x-ray emissions to be consistent with two-temperature thermal models, at temperatures of approximately $2.3 \times 10^6 K$ and $1.0 \times 10^7 K$.

This paper will examine the x-ray emissions from contact binary stars, using the ROSAT All-Sky Survey (RASS; Voges, et al. 1999), and a large new catalog of contact binaries (Gettel, et al. 2005). In section 2 we review the assembly of the contact binary catalog from ROTSE-I sky patrol observations. The rate of x-ray detections is discussed in sections 3.1 and 3.2, and we calculate the median x-ray luminosity of these systems in section 3.3. This is followed in section 4 by an analysis of the space density of contact binaries and an estimate of the contribution of contact binaries to the galactic x-ray background.

2. Assembly of the Contact Binary Catalog

The ROTSE-I robotic telescope obtained the optical variability data used in this work. ROTSE-I combined four Canon 200 mm f/1.8 lenses on a single mount, each of which was equipped with a 2048x2048 pixel Thompson TH7899M CCD. Each ROTSE-I pixel subtends $14.4''$ at this f-number. Designed to find optical counterparts to gamma-ray bursts, the telescope spent much of the time from March 1998 to December 2001 patrolling the sky. The combined array imaged a $16^\circ \times 16^\circ$ field of view, allowing it to image the entire sky twice each night, with two 80 s images each visit. The telescope was disassembled in 2002, but the lens and camera assemblies have been recycled as part of the Hungarian Automated Telescope Network (HAT-net Bakos, G., et al. 2004).

Initial studies of using ROTSE-I sky patrols for the detection of variable objects were reported in Akerlof, et al. (2000). This work examined only three months of data for just 5% of the sky patrol area, revealing nearly 1800 bright variable objects, most of which were previously unknown. More recently, Wozniak, et al. (2004) has completed reductions of a full year of ROTSE-I sky patrols, covering the entire region north of -30° declination, as part of the Northern Sky Variability Survey (NSVS). Details of the public release of this data are presented in Wozniak, et al. (2004).

The data amassed in the NSVS were used by Gettel, et al. (2005) to compile a new

catalog of contact binary stars. Details of the variable detection algorithms, light curve phasing, and contact binary identification are given there. A total of 1022 contact binaries are included in this catalog. Of these systems, over 800 were previously unidentified. The catalog was created through use of a known period-color relation for contact binary stars. Cuts were stringent, and the final catalog was checked by hand to ensure sample purity. This focus on purity had the unavoidable result of limiting the completeness of the catalog. Based on previous catalogs of contact binary systems, it is estimated that the new catalog is about 34% complete for contact binaries brighter than twelfth magnitude. Distances to cataloged systems were also calculated using a period-color-luminosity relation with J-H colors; the median distance to these systems is 380 pc. Errors in the distance estimates are generally around 20%.

3. X-ray Emission

To determine the incidence of x-ray emissions from contact binaries, we matched the new contact binary catalog to the RASS bright and faint source catalogs. The RASS was a complete sky survey, carried out using the ROSAT observatory between 1990 and 1991. Holes in the data were filled in during pointed observations in 1997, resulting in a complete all-sky survey. The scan path was 2 degrees wide and progressed along the ecliptic at a rate of 1 degree per day. Objects close to the ecliptic poles thus received a greater number of observations, and more cumulative observation time. Observations were made in the 0.1-2.4 keV energy band. More details concerning the RASS and the ROSAT observatory are documented in Voges, et al. (1999).

3.1. Determining the Incidence of X-ray Emission

We matched the RASS to the contact binary catalog using a $50''$ search radius. We choose this radius for the purposes of reducing spurious matches, and because more than 99% of objects in the RASS catalog have positional errors of less than $50''$. To check the abundance of false matches within the data set at this search radius, we created a catalog of random spacial points with a distribution similar to that of the NSVS catalog. This was accomplished by shifting each individual object in the contact binary catalog by random values between -5 and 5 degrees in both right ascension and declination. When we matched this randomized catalog with the ROSAT data using the same $50''$ search radius, we obtained an average of 3 spurious matches, or approximately 2.1% of detections.

In total, there were 140 matching x-ray sources out of the 1022 object contact binary catalog, at the 50'' radius. Of these matching objects, all had an optical magnitude brighter than 13.8. For further confirmation that the matches are not spurious, we searched the SIMBAD Astronomical Database¹ for other possible identifications of these ROSAT sources. Of these 140 RASS sources, the vast majority have not yet been classified. There were fifteen sources identified on SIMBAD as corresponding to a particular star, variable star, or W UMa type star. None of the listings in the database were inconsistent with contact binaries, though one source was listed as a β Lyrae type semi-detached contact binary system.

We use the distance estimates calculated in the contact binary catalog to account for the expected sensitivity loss due to distance. We find that out to an estimated distance of 200 parsecs, 61 of 102 contact binary systems have detectable x-ray emissions. This detection rate increases at closer distances, yielding 27 out of 35 systems closer than 150 pc, and close to a 100% detection rate out to 125 pc (15/16). The one contact binary not detected at this distance was not extraordinary in any way, save for it having the second longest period in the group. No matches were found when the estimated distance surpassed 550 pc. We can improve this detection rate by accounting for the variable sensitivity of the RASS.

Because of the increased exposure time near the ecliptic poles, there is also an increase in the sensitivity of the ROSAT data in that area. Figure 1 shows the minimum detected flux over one-degree strips of ecliptic latitude. Areas around the pole show as much as ten times the sensitivity of those in the ecliptic plane. Therefore, to best estimate the incidence of x-ray emission, we look at those objects which lie within 30 degrees of the ecliptic pole. This results in 41 RASS matches out of 174 total catalogued objects. In cutting out the ecliptic plane, there is effectively an increase in the general sensitivity of the RASS data, without an unacceptably large loss in sample size. There is a 100 percent detection rate for x-ray emissions in objects estimated to be within 180 pc and within 30 degrees of the ecliptic poles (12/12), and greater than 90% within 200 pc (16/17). The system not detected by the RASS has the faintest absolute magnitude (approximately 5.84) of any of the observed systems in this range, which could account for it not being detected.

Figure 2 shows the distribution of matches against all catalog objects, both before and after this cut. It is apparent that the actual detection rate begins to fall off after 200 pc, presumably due to the sensitivity of the RASS. The high detection rates strongly suggest that all contact binaries are significant sources of x-rays.

¹www.simbad.u-strasbg.fr/Simbad

3.2. Matching to Other X-ray Observations

Public data from the XMM-Newton Satellite (Jansen, et al. 2001) were also used to corroborate our results. Launched in December 1999, the XMM-Newton was scheduled for a two year mission of pointed observations, which was extended for another four years. Over the course of these pointed observations, numerous serendipitous sources were discovered. These were catalogued in The First XMM-Newton Serendipitous Source Catalogue (1XMM), XMM-Newton Survey Science Centre (2003). The catalog was compiled from 585 observations taken between March 2000 and May 2002, consisting of a net sky coverage of approximately 52 square degrees.

Again using a $50''$ search radius, we matched 1XMM to our catalog of contact binary systems. Two sources were found, one of which was observed on three separate occasions. To check the possibility that these are spurious matches, we employ the same procedure as for the RASS data. We find no matches using a randomized catalog, confirming that these sources are real matches. Both sources correspond to contact binaries in the catalog with magnitude fainter than 12.9, and are estimated to be greater than 550 pc distant (647 and 552 pc). This further confirms that all contact binaries are strong x-ray emitters, and those not detected by the RASS are missed because of sensitivity limits. Public data from the Chandra X-ray Observatory were also searched using a $1'$ search radius, but no overlapping observations were found.

3.3. Calculating X-ray Luminosity

For the 140 contact binaries matching RASS sources, we proceed to calculate the x-ray luminosities. To do this, it is necessary to convert the RASS count rate data into x-ray flux. For this purpose, we use the hardness ratio provided in the RASS data, defined by:

$$HR = \frac{H - S}{H + S} \quad (1)$$

where H denotes the source count in the hard passband (0.5–2.0 keV), and S denotes the source count in the soft passband (0.1–0.4 keV). This ratio allows us to convert the given count rates to x-ray flux (F_x), using the energy conversion factor of Hünsch, et al. (1996):

$$ECF = (5.3HR + 8.7) \times 10^{-12} \text{ erg cm}^{-2}\text{s}^{-1} \quad (2)$$

We expect that effects of interstellar absorption will be small for most of our sources,

due to their relative proximity. It should be noted that it is extremely difficult to quantify the error in ECF; we have consequently refrained from providing error estimates for our luminosities. Further, it is expected that the error in distance estimates will dominate the error in the final calculated luminosities. To get F_x , we multiply the source count rate by the calculated ECF. The total x-ray luminosity is then given by:

$$L_x = 4\pi d^2(F_x) \quad (3)$$

where d is the distance estimate provided in the catalog, and F_x is the calculated x-ray flux. Table 1 lists the x-ray data for each system, along with some other physical parameters.

The limits on the sensitivity of the RASS data are clearly evident when we plot luminosity versus distance (Figure 3). We can calculate an estimated detectable distance limit by taking the minimum hardness ratio to be -0.5, along with an estimated minimum count rate of 0.005 cts s⁻¹. We take 0.005 cts s⁻¹ as minimum, due to the fact that the lowest detected count rate among the contact binaries is 0.005027 cts s⁻¹. The minimum hardness ratio is estimated in a similar fashion. The detections closely follow this calculated distance limit, though it appears that the calculated limit overestimates the sensitivity of the RASS.

We calculate the x-ray luminosity distribution function for the x-ray detections estimated to be closer than 150 parsecs. We use only these detections due to the relatively high detection rate out to this distance. At greater distances, the sample becomes biased toward greater luminosities, because only the stronger emitters can be detected. The distribution function is given in Figure 4. From this distribution, we calculate the median x-ray luminosity to be $L_{x,median} = 10^{30.0}$ erg s⁻¹.

As previously stated, we refrain from providing detailed error estimates for our data, due to the inability to determine the error in the ECF. Errors in the distance estimates range from approximately 50% to as little as 10%. Assuming that the ECF is reasonably accurate, we expect that the errors in the luminosities thus range from 15% to 70%. We expect that all calculated luminosities have errors of less than a factor of two.

The x-ray luminosity was also calculated for the two XMM-Newton sources. The 1XMM lists the detections in terms of flux, rather than count rate, thus eliminating a step from the calculations above. For our purposes, we used the weighted total flux from all cameras aboard the satellite. For the source detected three separate times, we took the mean flux from all three detections. Using equation (3), we calculated the median luminosity of the 1XMM sources to be 1.2×10^{30} erg s⁻¹, i.e $\log L_{x,median} = 30.1$, which is consistent with our findings for the ROSAT sources. The x-ray data for these sources is summarized in Table 2.

4. Estimating the Volume Emissivity

Using the estimated distances, the volume density of the sample of contact binaries was determined in Gettel, et al. (2005). This was done by fitting the cumulative number of detected contact binaries versus distance (see Figure 5). The fitted curve is $N = (9.9 \pm 3.7) \times 10^{-6} d^3$. Accounting for the sky coverage of the catalog, this corresponds to an observed space density of $(5.7 \pm 2.1) \times 10^{-6} \text{pc}^{-3}$. This value is then adjusted to account for the catalog’s estimated 34% completeness, yielding a final completeness-adjusted space density of $(1.7 \pm 0.6) \times 10^{-5} \text{pc}^{-3}$. The cumulative number density distribution suggests that the completeness for contact binary detection begins to fall off beyond 300 pc. This estimate of the contact binary space density agrees with the most recent value published by Rucinski (2002), of $(1.02 \pm 0.24) \times 10^{-5} \text{pc}^{-3}$.

The x-ray volume emissivity is now calculated using the completeness-adjusted space density along with the mean calculated luminosity from the sample. We assume that each contact binary emits the mean flux, and calculate the flux per cubic parsec. The result is a flux density of approximately $(1.7 \pm 0.6) \times 10^{25} \text{erg s}^{-1} \text{pc}^{-3}$. This value is in agreement with the $1.3 \times 10^{25} \text{erg s}^{-1} \text{pc}^{-3}$ estimated by Stępień, et al. (2001), and is more than an order of magnitude smaller than the value derived for M dwarfs by Schmitt & Snowden (1990). We therefore conclude that the contribution of contact binaries to the galactic x-ray background is insignificant.

5. Conclusions

Due to the high RASS detection rate among the catalog of contact binaries, we conclude that, as expected, all such systems are significant sources of X-rays. The calculated median x-ray luminosity is in agreement with previous studies, such as that by Stępień, et al. (2001).

The volume emissivity of the contact binary systems is estimated at $(1.7 \pm 0.6) \times 10^{24} \text{erg s}^{-1} \text{pc}^{-3}$, which is not enough to account for any significant portion of the galactic x-ray background. This value is in agreement with the value published by Stępień, et al. (2001). Interestingly, we arrive at this similar value through a significantly lower median x-ray luminosity, but a higher calculated space density. The space density is, however, in line with other estimates, such as that of Rucinski (2002). Both the space density estimates and our estimates of x-ray luminosity are sensitive to distance estimates. If distances are underestimated, space densities rise and luminosities fall. This likely accounts for the agreement in volume emissivity measured here and in Stępień, et al. (2001). Regardless, the volume emissivity remains an insignificant contribution to the galactic x-ray background.

We have made use of the ROSAT Data Archive of the Max-Planck-Institut Für extraterrestrische Physik (MPE) at Garching, Germany. We have also made use of observations obtained with XMM-Newton, an ESA science mission with instruments and contributions directly funded by ESA Member States and NASA.

This research has made use of data obtained from the High Energy Astrophysics Science Archive Research center (HEASARC), provided by NASA's Goddard Space Flight Center. It has also made use of the SIMBAD database, operated at CDS, Strausbourg, France.

ROTSE is supported at the University of Michigan by NSF grants AST 99-70818, AST 97-03282, and AST 04-07061 NASA grant NAG 5-5101, the Research Corporation, the University of Michigan, and the Planetary Society.

REFERENCES

- Akerlof, C., et al., 2000, AJ, 119, 1901.
- Bakos, G., et al., 2004, PASP, 116, 266.
- Cruddace, R.G., & Dupree, A.K., 1984, ApJ, 277, 263
- Hünsch, M., Schmitt, J.H.M.M., Schröder, K.-P., & Reimers, D., 1996, A&A, 310, 801.
- Gettel, S., et al., 2005, submitted AJ
- Jansen, F., et al., 2001, A&A, 365, L1
- Lucy, L.B. 1968, AJ, 151, 1123
- McGale, P.A., Pye, J.P., Hodgkin, S.T., 1996, MNRAS, 280, 627
- Rucinski, S. 1992, AJ, 103, 960
- Rucinski, S., 2002, PASP, 114, 1124
- Schmitt, J.H.M.M., & Snowden, S.L., 1990, ApJ, 361, 207.
- Stępień, K., Schmitt, J.H.M.M., & Voges, W., 2001, A&A, 370, 157.
- Voges, W., et al., 1999, A&A, 349, 389.
- Wozniak, P., et al., 2004, AJ, 127, 2436.

XMM-Newton Survey Science Centre, 2003, The First XMM-Newton Serendipitous Source
Catalogue

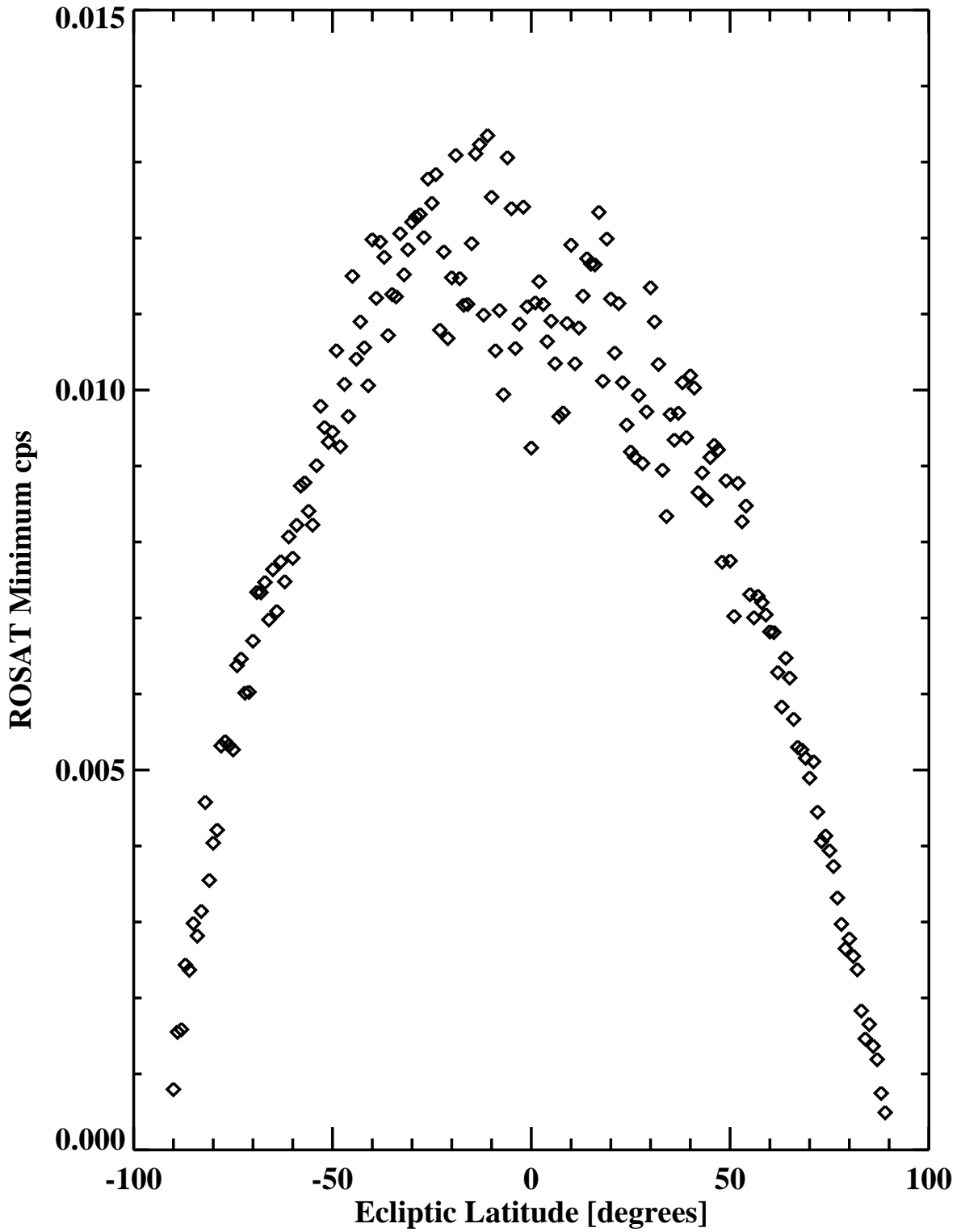


Fig. 1.— Dependence on ecliptic latitude of the RASS sensitivity. The minimum detected count rate is shown for one degree strips of ecliptic latitude. The great increase in sensitivity toward the ecliptic poles is obvious.

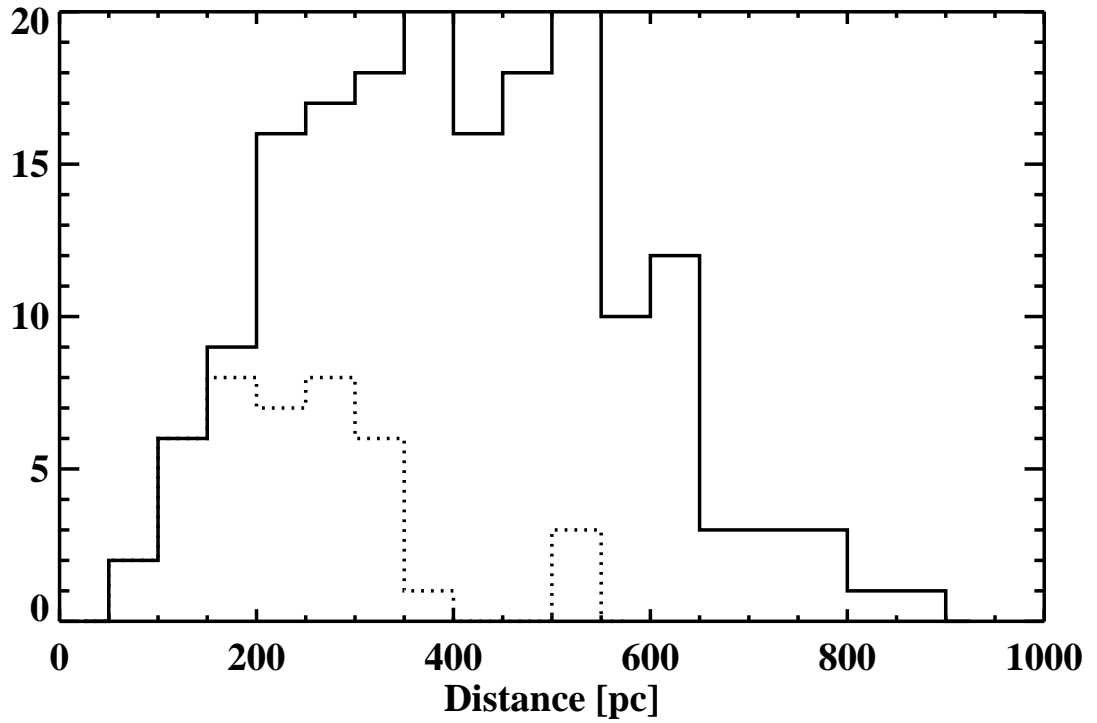
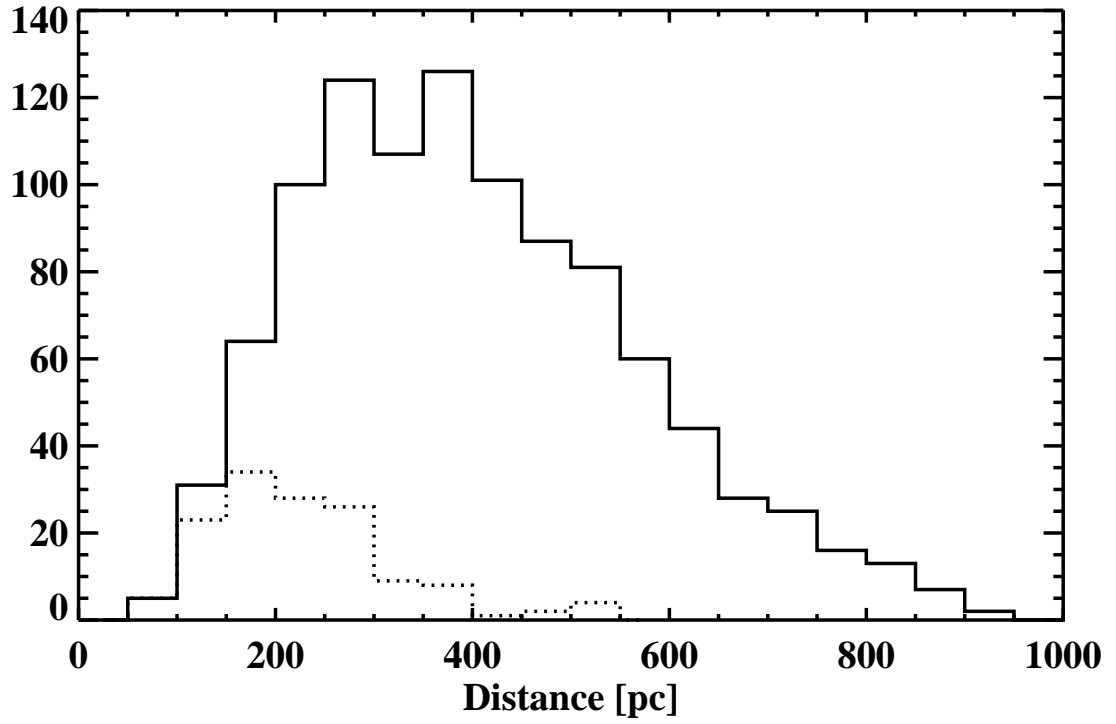


Fig. 2.— Top: Distribution of contact binaries over distance. The solid line represents all catalog objects, while the dotted line represents those objects matched to the RASS catalog. Bottom: Plot of the same distribution, after applying the cut around the ecliptic pole.

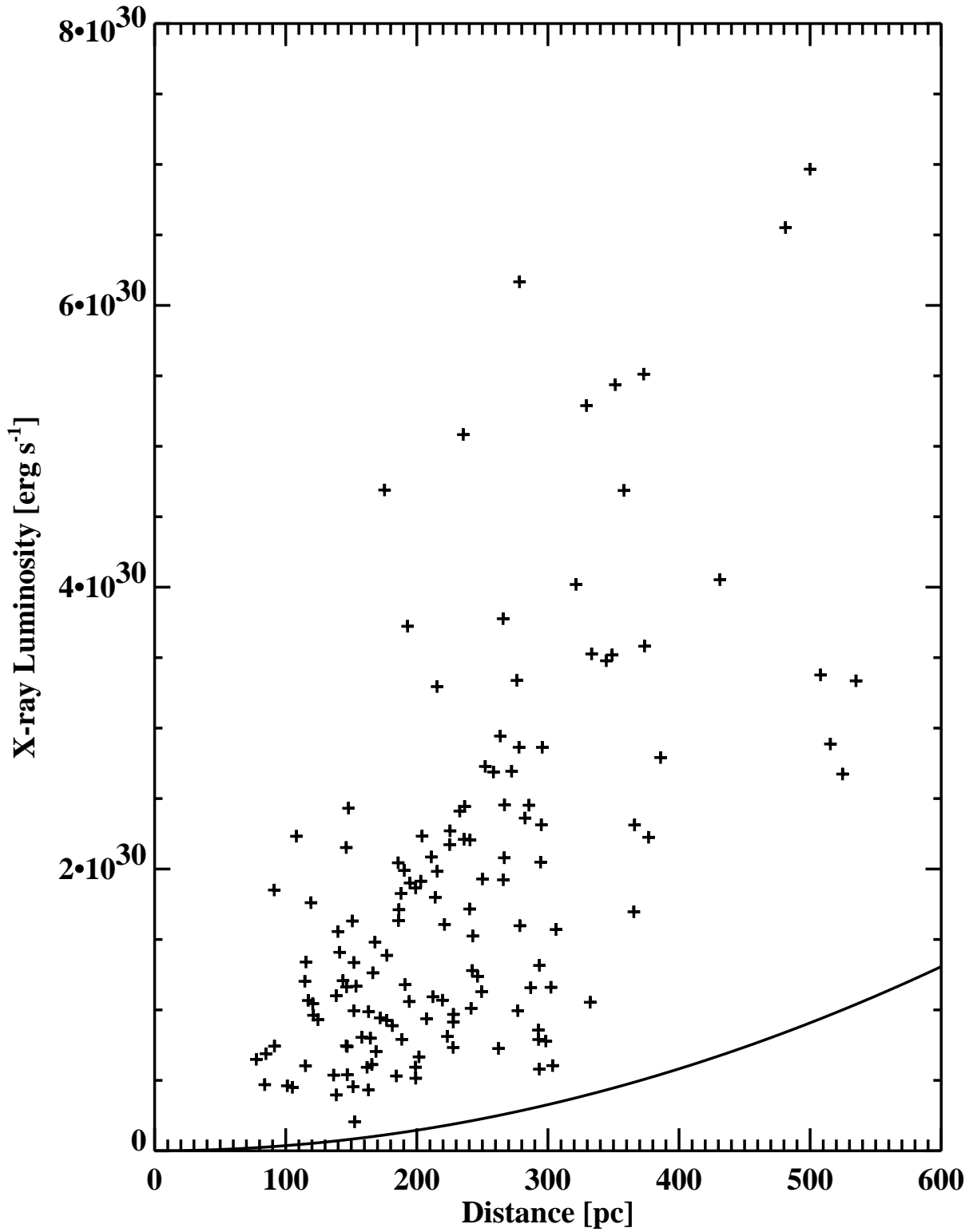


Fig. 3.— Distribution of calculated luminosities over distance. The pluses represent contact binary systems with matching RASS data. The solid line represents the estimated detectable flux limit for the ROSAT observations.

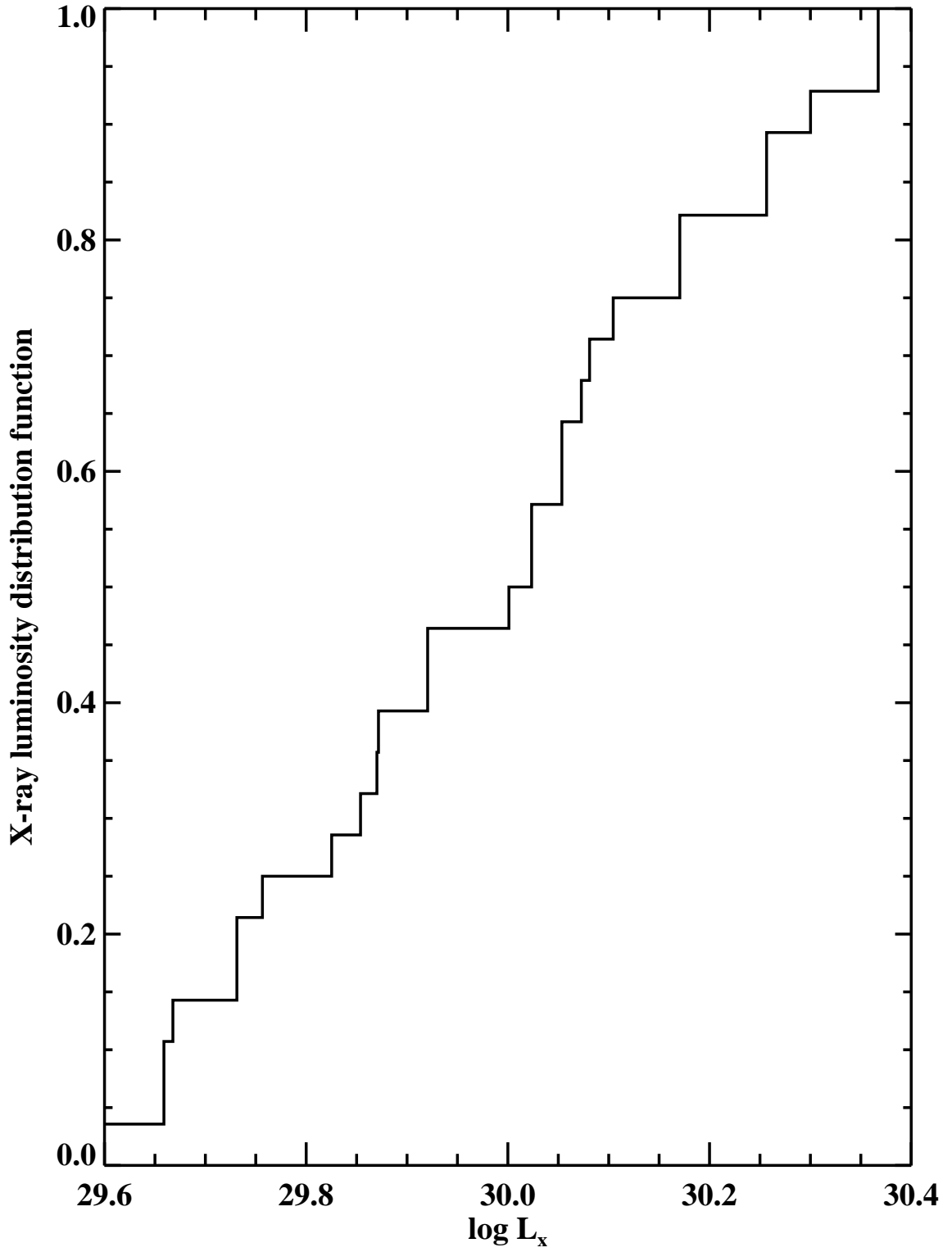


Fig. 4.— Observed x-ray luminosity distribution function for contact binaries within 150 pc.

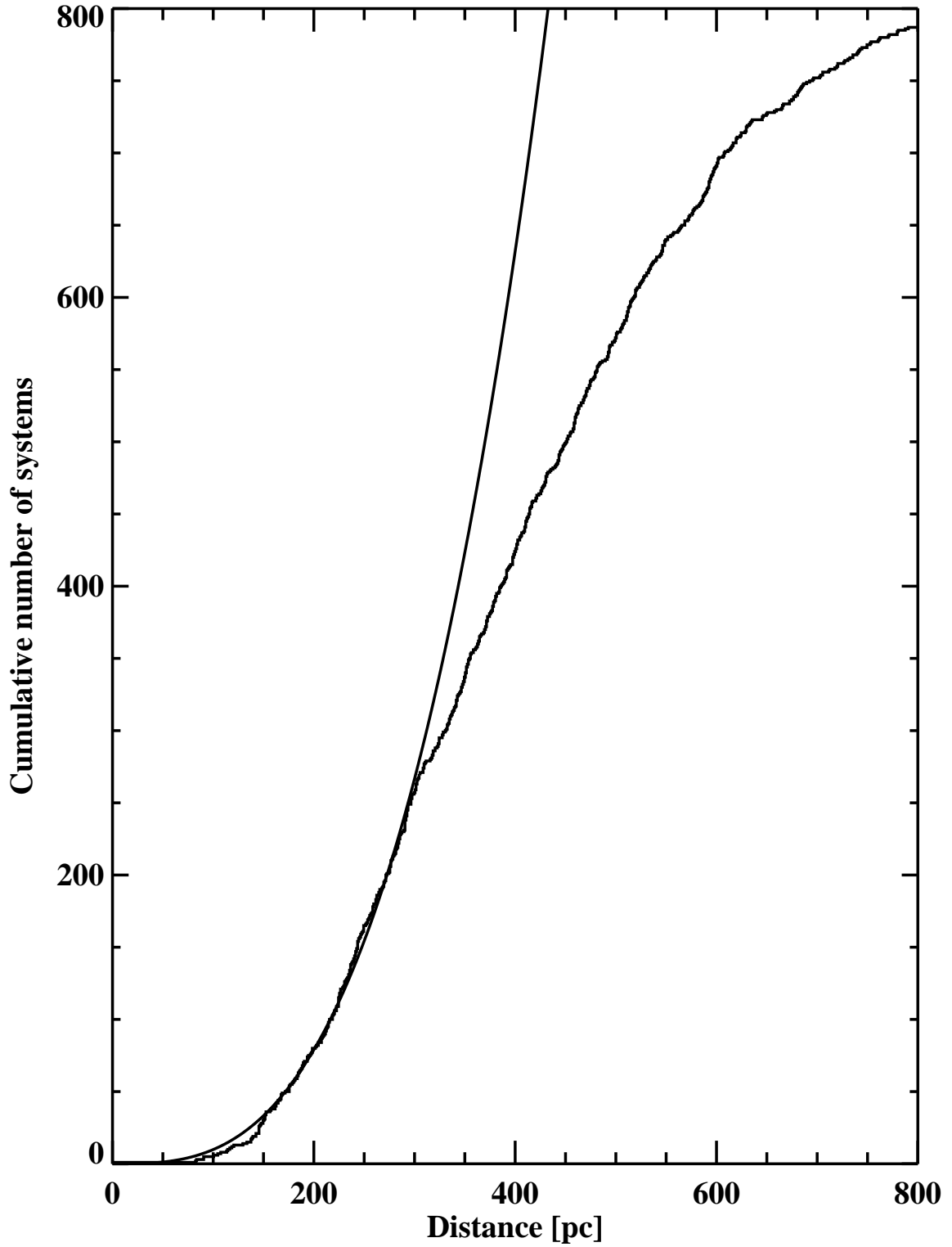


Fig. 5.— Cumulative number of systems as a function of distance. The smooth curve represents the curve $N = 9.9 \times 10^{-5}d^3$. The fit is very good out to about 300 pc.

Table 1. Properties of RASS objects in the contact binary catalog.

1RXS	RA ^a	Dec	P (days)	d (pc)	cts s ⁻¹	HR	$\log L_x$
1RXS J215434.0-100219	328.640	-10.0360	0.263045	250	0.02704	0.86	30.4
1RXS J111135.3-132604	167.895	-13.4360	0.263549	120	0.05249	0.16	30.0
1RXS J050837.5+051157	77.1518	5.20592	0.266356	120	0.07461	0.00	30.0
1RXS J125121.7+271359	192.840	27.2296	0.266683	230	0.01360	0.40	30.0
1RXS J160150.9+245213	240.473	24.8715	0.268739	190	0.01474	0.74	29.9
1RXS J085204.8-225942	133.020	-22.9970	0.272325	150	0.04776	0.15	30.1
1RXS J000637.5+552717	1.65577	55.4560	0.272491	80	0.09294	0.19	29.8
1RXS J172406.8+735439	261.026	73.9101	0.272885	180	0.01225	0.37	29.7
1RXS J144926.8+571803	222.365	57.2990	0.275180	90	0.09213	-0.12	29.9
1RXS J030425.8+061225	46.0986	6.19682	0.275376	240	0.01775	1.00	30.2
1RXS J085650.9+023040	134.211	2.50686	0.275415	150	0.02176	-1.00	29.3
1RXS J203556.9+490036	308.986	49.0129	0.278522	110	0.03968	-0.02	29.7
1RXS J123129.5+683752	187.889	68.6355	0.279921	200	0.01575	-0.14	29.8
1RXS J033959.1+031421	54.9961	3.24179	0.282723	150	0.03522	-0.08	29.9
1RXS J014726.3-170345	26.8556	-17.0660	0.282935	210	0.01984	0.09	30.0
1RXS J102555.0+204912	156.483	20.8210	0.284977	190	0.03115	-0.22	30.0
1RXS J145154.8+604616	222.987	60.7723	0.287049	150	0.02700	-0.18	29.7
1RXS J061531.4+193553	93.8817	19.5891	0.287835	200	0.03224	0.66	30.3
1RXS J115752.7+062658	179.463	6.45148	0.289806	210	0.04852	-0.12	30.3
1RXS J083947.9-042941	129.943	-4.49980	0.289942	280	0.05651	0.58	30.8
1RXS J164215.2+660711	250.566	66.1179	0.290370	290	0.007729	0.40	29.9
1RXS J203104.5+384709	307.773	38.7834	0.290625	160	0.01752	-0.18	29.6
1RXS J180818.5+343438	272.078	34.5767	0.291362	370	0.01600	-0.39	30.2
1RXS J114534.7+513056	176.402	51.5115	0.293847	270	0.02480	0.55	30.4
1RXS J180836.4+334202	272.149	33.7016	0.294283	240	0.01990	0.41	30.2
1RXS J050851.6+025000	77.2155	2.82084	0.295713	160	0.02597	0.61	30.0
1RXS J065822.0+364024	104.593	36.6777	0.295931	180	0.02346	0.35	30.0
1RXS J083757.6+554842	129.486	55.8064	0.298207	240	0.02670	0.61	30.3
1RXS J071659.2+771039	109.270	77.1739	0.298445	200	0.01156	0.13	29.7
1RXS J212351.2+633359	320.952	63.5578	0.298759	280	0.007736	1.00	30.0
1RXS J075735.4+265147	119.393	26.8641	0.299190	250	0.02403	-0.45	30.1
1RXS J145008.1+293859	222.533	29.6498	0.301604	170	0.01616	0.77	29.8
1RXS J164817.3+444430	252.065	44.7411	0.302027	220	0.01146	0.60	29.9

Table 1—Continued

1RXS	RA ^a	Dec	P (days)	d (pc)	cts s ⁻¹	HR	$\log L_x$
1RXS J183111.3+562459	277.793	56.4179	0.302035	300	0.01220	0.00	30.1
1RXS J034927.4+125454	57.3653	12.9112	0.305383	80	0.04858	0.52	29.7
1RXS J093201.5-133419	143.008	-13.5690	0.305816	200	0.03421	0.50	30.3
1RXS J061241.9-330909	93.1741	-33.1500	0.305952	350	0.02148	0.48	30.5
1RXS J153445.3+621655	233.688	62.2790	0.306712	150	0.01689	0.21	29.7
1RXS J174402.4+701527	266.001	70.2586	0.308014	140	0.02111	-0.10	29.6
1RXS J223616.7+060101	339.065	6.01434	0.309404	190	0.03707	0.49	30.3
1RXS J201859.2+563617	304.745	56.6054	0.311254	80	0.08370	0.16	29.8
1RXS J175255.4+752013	268.205	75.3386	0.312436	290	0.005027	0.47	29.8
1RXS J085524.0-162720	133.854	-16.4560	0.314788	290	0.01765	0.47	30.3
1RXS J172023.6+411510	260.099	41.2542	0.315415	270	0.01913	0.60	30.3
1RXS J014852.7-205340	27.2253	-20.8920	0.316859	120	0.07302	-0.09	30.0
1RXS J002827.8+785750	7.11603	78.9620	0.317412	170	0.04132	0.36	30.2
1RXS J071403.3-272509	108.521	-27.4250	0.318374	200	0.02327	-0.53	29.8
1RXS J004552.1+630456	11.4692	63.0853	0.318876	160	0.02633	0.29	29.9
1RXS J184509.7+284100	281.298	28.6889	0.318936	120	0.05522	0.23	30.0
1RXS J171240.3+330822	258.164	33.1334	0.320740	430	0.01974	0.10	30.6
1RXS J143214.4+173955	218.060	17.6657	0.322648	250	0.01219	1.00	30.1
1RXS J223616.0+331909	339.070	33.3158	0.322996	150	0.05357	0.47	30.2
1RXS J133100.8+413535	202.751	41.5950	0.323628	220	0.01962	1.00	30.2
1RXS J163219.7+775422	248.067	77.9038	0.324269	370	0.01172	0.68	30.4
1RXS J231948.3+360408	349.952	36.0641	0.325102	260	0.02902	0.66	30.5
1RXS J171413.9+764215	258.558	76.7040	0.325397	170	0.01899	0.21	29.8
1RXS J150109.4+484805	225.290	48.8044	0.326787	340	0.02430	0.26	30.5
1RXS J124338.0+384404	190.905	38.7374	0.326893	150	0.02909	0.22	29.9
1RXS J162743.9+564557	246.934	56.7662	0.329333	260	0.009346	0.14	29.9
1RXS J042812.5+530308	67.0569	53.0457	0.329920	190	0.03537	1.00	30.3
1RXS J183336.5+463602	278.401	46.5960	0.330258	300	0.005529	0.23	29.8
1RXS J173840.5+211854	264.666	21.3137	0.332446	230	0.01113	1.00	30.0
1RXS J024553.4+342848	41.4744	34.4916	0.332618	360	0.02680	0.51	30.7
1RXS J192104.3+561940	290.268	56.3281	0.334292	230	0.03539	0.27	30.3
1RXS J035159.7-215521	58.0009	-21.9300	0.335169	270	0.02779	0.42	30.4
1RXS J184140.3-004455	280.413	-0.745600	0.335915	290	0.01796	1.00	30.4

Table 1—Continued

1RXS	RA ^a	Dec	P (days)	d (pc)	cts s ⁻¹	HR	$\log L_x$
1RXS J035228.5+833154	58.1789	83.5398	0.337919	220	0.01366	0.92	30.0
1RXS J093124.1-045939	142.853	-4.99780	0.339773	170	0.03194	0.61	30.1
1RXS J174358.1+341814	265.988	34.3007	0.340097	210	0.01738	0.56	30.0
1RXS J213852.7+280532	324.717	28.0961	0.341936	290	0.01476	-0.01	30.1
1RXS J141726.6+123354	214.358	12.5674	0.342325	140	0.05328	0.09	30.1
1RXS J053843.7-082001	84.6880	-8.33300	0.344259	280	0.01802	0.16	30.2
1RXS J005328.9+253630	13.3671	25.6065	0.345575	240	0.05517	0.98	30.7
1RXS J171112.8+683332	257.801	68.5564	0.347222	290	0.006420	0.62	29.9
1RXS J201224.5+095919	303.105	9.98977	0.348206	250	0.01885	0.94	30.3
1RXS J193429.5+740225	293.640	74.0517	0.350340	330	0.009349	-0.03	30.0
1RXS J093547.4-133455	143.946	-13.5850	0.351053	180	0.1014	0.73	30.7
1RXS J173936.5+501207	264.906	50.2005	0.352265	520	0.008227	0.22	30.4
1RXS J204010.1+635929	310.016	63.9921	0.352281	230	0.009211	0.78	29.9
1RXS J145627.9+462146	224.119	46.3621	0.352414	190	0.03414	0.54	30.2
1RXS J132735.1+030206	201.887	3.04122	0.353995	240	0.03160	0.54	30.4
1RXS J071922.9+415710	109.853	41.9517	0.355754	390	0.01687	0.11	30.4
1RXS J205711.4+125927	314.300	12.9927	0.357639	280	0.01766	1.00	30.4
1RXS J153648.4+473727	234.205	47.6220	0.360470	310	0.01320	0.36	30.2
1RXS J231714.8+365522	349.311	36.9183	0.360632	530	0.01080	0.06	30.5
1RXS J173327.4+265549	263.366	26.9298	0.360855	240	0.01328	0.42	30.0
1RXS J220745.6+304959	331.924	30.8339	0.360873	500	0.01935	0.63	30.8
1RXS J161520.0+354218	243.834	35.7073	0.360938	330	0.03135	0.81	30.7
1RXS J232933.9-034601	352.388	-3.76950	0.363668	300	0.01956	1.00	30.5
1RXS J210905.1+625331	317.282	62.8889	0.364383	100	0.04731	-0.14	29.7
1RXS J050111.5+343032	75.2951	34.5072	0.366360	150	0.03452	1.00	30.1
1RXS J093436.6+204316	143.661	20.7170	0.366845	280	0.02563	0.64	30.5
1RXS J205532.1-043057	313.886	-4.51550	0.366920	190	0.03963	0.32	30.2
1RXS J140146.1+320840	210.444	32.1466	0.366986	190	0.03937	0.43	30.3
1RXS J225804.8+805226	344.483	80.8686	0.368748	220	0.03204	0.46	30.3
1RXS J175532.1+434808	268.899	43.8056	0.369881	510	0.01165	0.13	30.5
1RXS J170121.5+420939	255.341	42.1640	0.370156	110	0.06974	0.43	30.1
1RXS J134908.2+201118	207.298	20.1903	0.370575	240	0.02560	-0.30	30.1
1RXS J130610.8+205625	196.548	20.9389	0.371087	190	0.03391	0.91	30.3

Table 1—Continued

1RXS	RA ^a	Dec	P (days)	d (pc)	cts s ⁻¹	HR	<i>logL_x</i>
1RXS J212125.1-030936	320.353	-3.16040	0.374463	120	0.06546	0.78	30.1
1RXS J004859.7-371812	12.2382	-37.3090	0.375057	370	0.02365	1.00	30.7
1RXS J182912.6+064717	277.304	6.78725	0.375325	150	0.06252	0.90	30.3
1RXS J100344.3+281400	150.934	28.2324	0.376121	150	0.09573	0.19	30.4
1RXS J084002.3+190017	130.007	19.0003	0.382892	150	0.03664	0.21	30.0
1RXS J015112.9+434904	27.8019	43.8189	0.383036	220	0.04237	1.00	30.5
1RXS J144351.3+474303	220.963	47.7174	0.387695	90	0.1845	0.26	30.3
1RXS J152407.9+691241	231.005	69.2073	0.390680	300	0.007068	0.31	29.9
1RXS J121034.4+631231	182.644	63.2030	0.396061	290	0.01862	-0.45	30.1
1RXS J131743.0-003341	199.429	-0.562800	0.398509	140	0.02786	-0.01	29.7
1RXS J170731.0+280222	256.881	28.0420	0.398569	120	0.09956	0.32	30.2
1RXS J065127.2+543231	102.852	54.5481	0.399131	270	0.03453	0.80	30.6
1RXS J123048.8+832257	187.664	83.3855	0.399592	240	0.02921	0.50	30.3
1RXS J182214.2+211053	275.560	21.1821	0.401067	480	0.01689	1.00	30.8
1RXS J001555.3+064456	3.98193	6.74591	0.401179	290	0.01618	0.95	30.4
1RXS J014131.4+093240	25.3824	9.54392	0.402266	280	0.02611	1.00	30.5
1RXS J233116.9-052239	352.820	-5.37130	0.403318	260	0.02403	1.00	30.4
1RXS J020418.9+235959	31.0767	24.0004	0.405989	230	0.02937	0.76	30.4
1RXS J172427.0+641224	261.112	64.2063	0.407497	160	0.01670	0.49	29.8
1RXS J180920.6+090907	272.339	9.15108	0.409006	110	0.1194	0.88	30.3
1RXS J080607.4+300815	121.527	30.1482	0.412940	350	0.02629	1.00	30.7
1RXS J063041.8-174854	97.6809	-17.8140	0.414329	180	0.01613	1.00	29.9
1RXS J002328.2-204151	5.86661	-20.6970	0.414655	140	0.05258	0.48	30.1
1RXS J090324.6+380602	135.850	38.0985	0.414935	140	0.06314	-0.21	30.0
1RXS J222214.1+263148	335.556	26.5340	0.415291	370	0.01691	0.75	30.6
1RXS J232216.6+725505	350.600	72.9158	0.417444	270	0.01746	1.00	30.3
1RXS J160602.0+501124	241.510	50.1866	0.419036	180	0.04027	0.09	30.1
1RXS J030744.8+365159	46.9390	36.8692	0.419983	170	0.02774	0.17	30.0
1RXS J143230.5+504944	218.127	50.8280	0.420508	140	0.06401	0.32	30.2
1RXS J180530.0+694506	271.376	69.7541	0.424028	190	0.02521	0.38	30.1
1RXS J052126.5+161348	80.3568	16.2226	0.430693	230	0.02972	0.72	30.4
1RXS J054301.6+683952	85.7711	68.6687	0.434166	200	0.03645	0.68	30.3
1RXS J145617.3+040218	224.067	4.04021	0.436878	320	0.02587	0.73	30.6

Table 1—Continued

1RXS	RA ^a	Dec	P (days)	d (pc)	cts s ⁻¹	HR	$\log L_x$
1RXS J205451.0-060152	313.709	-6.02710	0.438638	380	0.01929	-0.36	30.3
1RXS J053929.9-080855	84.8732	-8.14870	0.443992	160	0.01762	1.00	29.9
1RXS J030952.6-065327	47.4697	-6.89310	0.445283	190	0.05970	1.00	30.6
1RXS J233001.8-115421	352.508	-11.9080	0.445560	150	0.04642	0.04	30.1
1RXS J141447.2+680442	213.697	68.0784	0.458568	210	0.03035	0.40	30.3
1RXS J155445.4+854004	238.695	85.6685	0.488961	520	0.008693	0.33	30.5
1RXS J044237.9+725838	70.6928	72.9782	0.498355	120	0.05442	-0.32	29.8
1RXS J181550.6+410622	273.957	41.1090	0.528820	330	0.02578	0.30	30.5

^aRA and Dec information are taken from the corresponding NSVS observations, due to the better spacial resolution

Table 2. Properties of contact binaries detected in 1XMM

1XMM	RA	Dec	P (days)	d (pc)	$\log L_x$
1XMM J123730.2+260458	189.376	26.0825	0.3568	650	30.2
1XMM J150439.3+102522	226.164	10.4230	0.3549	550	29.9 ^a
1XMM J150439.3+102523	226.164	10.4226	0.3549	550	29.9
1XMM J150439.4+102524	226.164	10.4228	0.3549	550	29.8

^aThe last three systems are duplicate observations of the same star. The average of the three luminosities was used in calculating the median luminosity